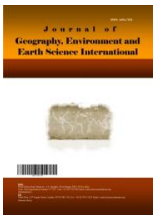

Journal of Geography, Environment and Earth Science International

23(4): 1-14, 2019; Article no.JGEESI.52971
ISSN: 2454-7352

A Spatial and Temporal Analysis of Atmospherics Parameters Retrieved by a Neuro-varationnal Method off the West African Coast

Daouda Diouf[1*], Sylvie Thiria[2], Awa Niang[1], Julien Brajard[2] and Michel Crepin[2]

[1]Laboratoire de Traitement de l'Information - ESP, Université Cheikh Anta Diop de Dakar, Sénégal.
[2]Laboratoire d'Océanographie et du Climat: Expérimentation et Approches Numériques, Université Pierre & Marie Curie, France.

Authors' contributions

This work was carried out in collaboration among all authors. Author DD designed the study, performed the statistical analysis, wrote the protocol and wrote the first draft of the manuscript. Authors ST, AN and MC managed the analyses of the study. Author JB managed the literature searches. All authors read and approved the final manuscript.

Article Information

DOI: 10.9734/JGEESI/2019/v23i430177
Editor(s):
(1) Dr. Wen-Cheng Liu, Department of Civil and Disaster Prevention Engineering, National United University, Miaoli Taiwan.
Reviewers:
(1) A. Ayeshamariam, Khadir Mohideen College, India.
(2) Peter Stallinga, University of the Algarve, Portugal.
(3) Mandadapu S. V. K. V. Prasad, Jawaharlal Nehru Technological University, India.
(4) Benjamin Chukwumah Anwadike, National Open University of Nigeria, Nigeria.
Complete Peer review History: http://www.sdiarticle4.com/review-history/52971

Original Research Article

Received 20 September 2019
Accepted 28 November 2019
Published 05 December 2019

ABSTRACT

In this work, we study spatial and temporal atmospherics parameters evolution retrieved by neuro-variationnal method from SeaWiFS observations measured off the west African coast.
The SeaWiFS sensor measures the radiance above the top of atmosphere (TOA) solar irradiance. SeaWiFS use standard algorithm to invert the signal in order to retrieve weakly absorbing aerosol optical thickness (*AOT*) less than 0.3 whereas the Senegalese coasts are frequently crossed by desert dust plumes from large optical thickness.
A neural algorithm, so-called SOM-NV, was developed to deal with absorbing aerosols and to retrieve their optical parameters, off the Senegalese coast, from SeaWiFS observations.
The impact of meteorological variables on these restitutions was studied over the entire period of

**Corresponding author: E-mail: dadiouf2001@yahoo.fr;*

the observations that we analyzed and over the whole studied area, on the one hand, but also in a more thorough way on three "sub-area" located in north, south and center. The results obtained showed that the composition of aerosols in the atmosphere is a function of the seasons. High altitude zonal U winds are correlated with non-desert aerosols of -62.16% in winter and autumn. The correlation is -60.32% between dust aerosols and the zonal wind.

Keywords: Kohonen map; neural network; SeaWiFS sensor; atmospherics parameters.

1. INTRODUCTION

Scattering of atmospheric aerosols and molecules disturb the observation of ocean color from space, and requires the use of an algorithm called atmospheric correction. Usual algorithms are non-absorbing aerosols assumption.

The determination of an aerosol model, namely its spectral dependence and the amount of aerosols is done by estimating the aerosol reflectance in one or more spectral bands in the near infrared, where the reflectance of the ocean is null because of its strong absorption at these wavelengths. By extrapolating the visible wavelengths estimated aerosol reflectance in the near infrared; we can then assess the marine reflectance at shorter wavelengths [1].

The observations by space-based sensors such as SeaWiFS showed that these assumptions are inadequate, especially for areas overflown by plume of desert dust (West Africa, Mediterranean).

Plumes of absorbing aerosols are observed regularly on the coast of West Africa near the Sahara. These mineral dusts have the distinction of being transported over long distances, and previous work showing that plumes of absorbing aerosols over the oceans have optical thicknesses of an order of magnitude larger than typically encountered in aerosol maritime conditions [2,3]. The absorbing aerosols affect particularly the visible wavelengths, absorption is much stronger at shorter wavelengths (blue and ultraviolet) [4]. The measurement of reflectance at the top of the atmosphere in the near infrared does not distinguish weakly or strongly absorbing aerosols [5], causing significant errors found on marine reflectance from space. In his thesis, [6] showed that the standard SeaWiFS algorithm does not correct the absorbing aerosols. The detection of absorbing aerosols requires the use of visible band. However, the reflectance of the ocean in the visible varies considerably with changes in various constituents of the water making it difficult to detect changes in reflectance due to atmospheric absorption of aerosols. In the blue (400-490), the absorption of aerosols but also phytoplankton is too high. Further in the green (around 555 nm), absorption of phytoplankton is minimal but with strong backscattering effects, reflectance increases with the increase of chlorophyll.

The 510 nm band is the one for which the effects of absorbing aerosols are not high but also the reflectance of the sea varies little with the chlorophyll [7].

2. DATA USED

2.1 Study Area

Our study area is located off the West African coast in an area between 8°–24°N and 14°–30°W. We also targeted sub-areas in the north, south and center for a more local study. Sub-area 1 has coordinates 22-20°W and 12-14°N, sub-area 2, 28-26°W and 15-17°N and sub-area 3 is between 22-20°W and 20-22°N. Each sub-area is 220 km x 220 km.

2.2 SeaWiFS Measurements

The SeaWiFS provides 8 daily luminance measurements (*L*) in the visible at 412 nm, 443 nm, 490 nm, 510 nm, 555 nm, 670 nm) and near infrared, 765 and 865 nm, dedicated to atmospheric corrections. SeaWiFS Project radiances level L1A GAC are acquired free from the Goddard Space Flight Center. At each wavelength is calculated reflectance ρ corresponding to a radiance L:

$$\rho(\lambda,\theta_v,\varphi)=\frac{\pi\cdot L(\lambda,\theta_v,\varphi)}{E_0(\lambda)\cdot\cos(\theta_s)} \quad (1)$$

where $E_0(\lambda)$ is the extraterrestrial solar irradiance, θ_S , θ_V are the sun and satellite viewing zenith angles, respectively, and φ is the azimuth angle.

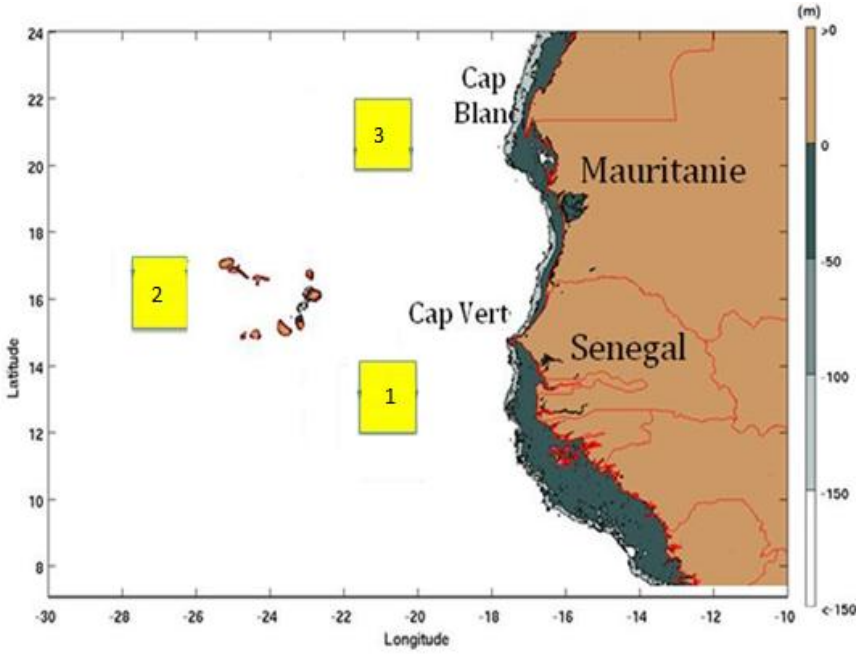

Fig. 1. Zone maps for the analysis of correlations between meteorological parameters and atmospheric SOM-NV products. Sub-area (Yellow Square) are situated at north, center, and south

$\rho_{toa}(\lambda)$ reflectance measured by a radiometer is the sum of contributions to the signal of each constituent of the atmosphere and ocean: $\rho_A(\lambda)$, is the reflectance resulting from multiple scattering of aerosols in the absence of the air ρ_a together with the combined aerosols/molecules in the atmosphere ρ_{ra} ; $\rho_q(\lambda)$, the reflectance due to specular reflection of sunlight on the sea surface; ρ_{wc} (λ), is the reflectance due to white caps; ρ_w (λ), is the contribution of the water. It corresponds to photons which, after penetrating the sea surface, are released and return to the sensor. This reflectance contains information on the ocean constituents near the ground.

$$\rho_{toa}(\lambda) = \rho_r(\lambda) + \rho_A(\lambda) + T(\lambda).\rho_g(\lambda) + t(\lambda).\rho_{wc}(\lambda) + t(\lambda).\rho_w(\lambda) \quad (2)$$

where $T(\lambda)$ the direct transmittance, $t(\lambda)$ is the transmittance of the atmosphere at a given wavelength (λ) [5,8].

The contribution of Rayleigh, specular reflection and absorption gas are known a priori with accuracy and have been removed from the signal. Also the pixels of land and clouds were eliminated. In fact we used the algorithm for detecting clouds [9], which is to reject pixels which ρ_{cor} (865) > 0.4 and those whose spatial variance calculated over a 3x3 neighborhood is greater than 5.10^{-4}.

Thus the corrected reflectance is:

$$\rho_{cor} = \rho_A + t.\rho_w \quad (3)$$

It is assumed that for the corresponding wavelengths to the near infrared (λ> = 670) the ocean is black, i.e, there is no light reflected. This is equivalent to ρ_w (λ>=670)=0. In fact for these wavelengths, the reflectance ocean ρ_w is minimal compared to the atmospheric reflectance. However, even if this hypothesis is true in most cases, it often remains a residual marine signal at 670 nm that is not negligible. Moreover, some chlorophyll rich waters or case 2 waters do not verify this hypothesis.

From these SeaWiFS images, we have created a training database so-called $Data^{obs}$. The $Data^{obs}$ length is 426,117 in size 10, it consists of eight corrected reflectances at wavelengths measured channels 413 nm, 443 nm, 490 nm, 510 nm, 555 nm, 665 nm, 765 nm, 865 nm and two angles: θ_S and γ who is the scattering angle. The scattering angle can better describe the geometry of observation since it includes the azimuthal difference.

$$\cos(\gamma) = -\cos(\theta_S)\cos(\theta_V) - \sin(\theta_S)\sin(\theta_V)\cos(\Delta\varphi)$$

This database has been normalized over a range of [0 1] by:

$$x_{norm} = \frac{x - \min(X)}{\max(X) - \min(X)} \quad (4)$$

Where x_{norm} the normalized value, min (X) and max (X) respectively the minimum and maximum of the sample.

Theoretical database $Data^{expert}$ or LUT (Look-Up-Table), which bind examples of relationship reflectance-parameters of the ocean and/or reflectance-atmospheric parameters, exist. They were generated using the radiative transfer codes.

This LUT contains parameters such as: type of aerosol, aerosol optical thickness at 865 nm, solar zenith angle θ_S, the zenith angle θ_V, the azimuthal difference $\Delta\varphi$, and the theoretical spectra of luminance at wavelengths (nm) 412, 443, 490, 510, 555, 665, 765, 865.

This database contains near 12 million simulations based on five models including four from the aerosol radiative transfer model with two layers [10] and based on [11], and one absorbing type [9]. All five are in relative humidity (RH) of 70%, 80%, 90%, 99%. The four models [11] are Maritime, Oceanic, Coastal and Tropospheric. The African dust model represents the absorbing type.

The aerosol models are defined by physical and chemical properties:

- The Rural model: A mixture of 70% water solution (mainly ammonium sulphate, calcium, and organic compounds) and 30% of dust-like (similar to dust particles). The modal radius r_1 of the small particles varies between 0.027 and 0.05215 μm when Relative Humidity (RH) varies from 0-99%. The coarse particles r_2 ranges from 0.43 to 1.1755 μm when RH varies from 0-99%.
- The Maritime model: It is composed of sea salt (mainly sodium chloride) and a continental type which can be likened to an aerosol rural model with the exception of these large particles were removed by the masses air blowing off the ocean. Its modal radius varies from 0.16 to 0.75 μm for RH ranging from 0-99%.
- The Oceanic model: It is an extreme case of the maritime model. The mode of particles is large and they are mainly composed of sea salt.
- The Tropospheric model: As the name suggests, it is located aerosols in the free troposphere (the layer above the limit) except that the particles whose radius is greater than 0.05 μm are excluded.
- The Coastal model: It has been defined by [1] and simulates situations that may be encountered near the coast. It is a mixture of rural and maritime models of [11].
- The African dust model: It is proposed by [9]. These models simulate the situations of dust traversing the West Africa coast. It is highly absorbing and often characterized by high optical thickness.

$Data^{expert}$ was used in order to introduce the expertise and to retrieve the aerosol type and the optical thickness values.

The meteorological data come from the new ERA-Interim re-analysis of the European Center for Medium-Range Weather Forecasts (ECMWF).

The spatial resolution is 0.75° and for the temporal resolution, the numerical model assimilates the observations every 6 hours (00:00, 06:00, 12:00, 18:00 UTC): the meteorological variables calculated by the so-called variables analyzed are stored four times a day. For each day and for each meteorological variable, the average of these 4 data stored every day is averaged to obtain the daily value. This allows thereafter to have the weekly average, monthly as well as the total average of all the data of a certain parameter.

The analyzed data consist of dynamic and thermodynamic variables such as pressure, temperature, precipitable water, wind speed, specific and relative humidity, etc.

3. METHODS

In this study, we used SOM-NV [12] that is a-two successive models for analyzing the $Data^{obs}$ images; the Self Organizing Map (SOM, [13]) model and the NeuroVaria method [14,6].

3.1 Labeling Phase

The vectors of $Data^{obs}$ were clustered into 600 groups of (reflectance; angle). We denoted this topological map as SOM-A-S (SOM-Angle-Spectrum). In the light of the results obtained by

[15], we chose a similar architecture for SOM-A-S: a two-dimensional array with a large number of neurons (20 x 30 = 600). The spectra of $Data^{expert}$ were associated with those of the neurons of SOM-A-S. At the end of the process, we obtained a SOM-A-S map that can be labeled by the physical parameters: *AOT* and aerosol type, associated with the neurons which had captured the $Data^{expert}$ vectors.

3.2 Decoding Phase

Pixels captured by a neuron were assigned to the aerosol type and aerosol optical thickness (*AOT*) associated with this neuron during the labeling phase.

The NeuroVaria algorithm provided accurate atmospheric corrections for inverting satellite ocean colour measurements; we use the atmospheric parameter values given by SOM-A-S as first guesses for NeuroVaria.

NeuroVaria provide accurate atmospheric corrections for inverting satellite ocean-colour measurements. The algorithm minimizes a weighted quadratic cost function, *J*, by adjusting control parameters (atmospheric and oceanic) such as *AOT* and C [16]. *J* describes the difference between the satellite measurement robs and a simulated reflectance computed using radiative transfer codes modelled by supervised neural networks (the so called Multi-Layer-Perceptrons, MLP). The minimization implies the computation of the gradient of *J* with respect to the control parameters and consequently of the derivatives of the MLPs, which is done by the classical gradient back-propagation algorithm [17]. On this version of SOM-NV, the MLPs modelling the radiative transfer codes were specially designed to take African dusts into account.

The complete methodology was applied to SeaWiFS images of the ocean off the West African coast from 1997 to 2009 to produce the type of aerosol, the *AOT*.

Monthly mean maps aerosols were calculated on 9 km x 9 km used for SEAWIFS GAC product level-3. Seasonality strong *AOT*(865) is characterized by a strong invasion of dust into the months of June, July, August. Their intensities vary from year to year, depending on aridity conditions in Africa and the wind direction.

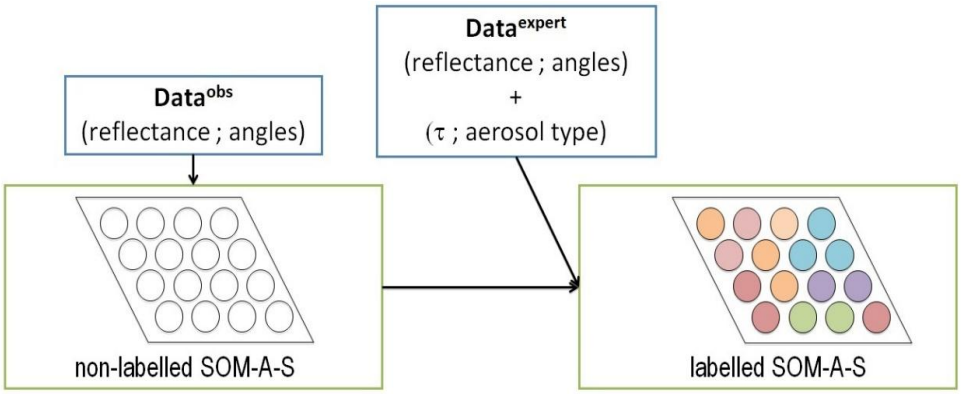

Fig. 2. SOM-NV: Labelling phase

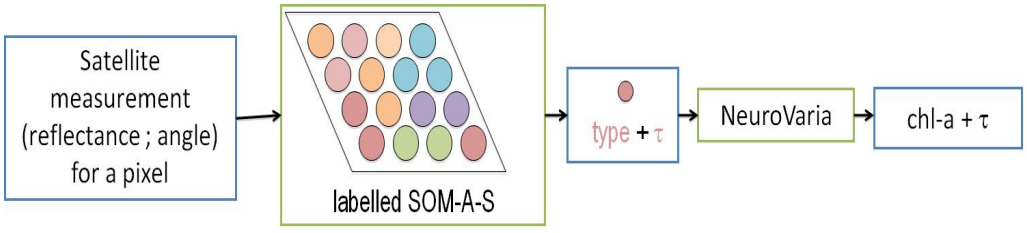

Fig. 3. SOM-NV: Decoding phase

4. RESULTS

4.1 Monthly Aerosol Optical Thickness Analysis

Monthly mean of Aerosols optical thickness was calculated from the data retrieved by SOM-NV and SeaWiFS standard algorithm. The SeaWiFS processing does not take into account values of *AOT* exceeding 0.35, which may bias the calculation of the optical thickness averages. The invasion of the Atlantic by desert dust is an event whose intensity peaks in June, July and August. This intensity varies according to the year, depending on the drought conditions in Africa and the speed and direction of the winds. For example in Fig. 4, there are strong optical thicknesses in June (usually > 0.5) and low optical thicknesses in November. This seasonal variability is observed from one year to the next.

The aerosol optical thickness provided by the AERONET [18] database are calculated monthly between January 1998 and December 2009 at the Dakar and Cape Verde stations from specific radiometers located at each of the stations.

In order to compare the satellite measurements with those made at the two AERONET stations, we have established collocated between satellite measurements and AERONET. Figs. 5 and fig. 6 represent the scatter plots of the monthly averages of *AOT* retrieved by SOM-NV and SeaWiFS according to *AOT* measured by AERONET respectively in Dakar and Cape Verde. Performance in terms of correlation and relative error are summarized in Table 1 and Table 2. The correlation of SOM-NV with AERONET is much better than that of SeaWiFS with AERONET, which is not significant. At the same time, there is a relative error of SOM-NV (~40%) very much lower than that of SeaWiFS (>60%).

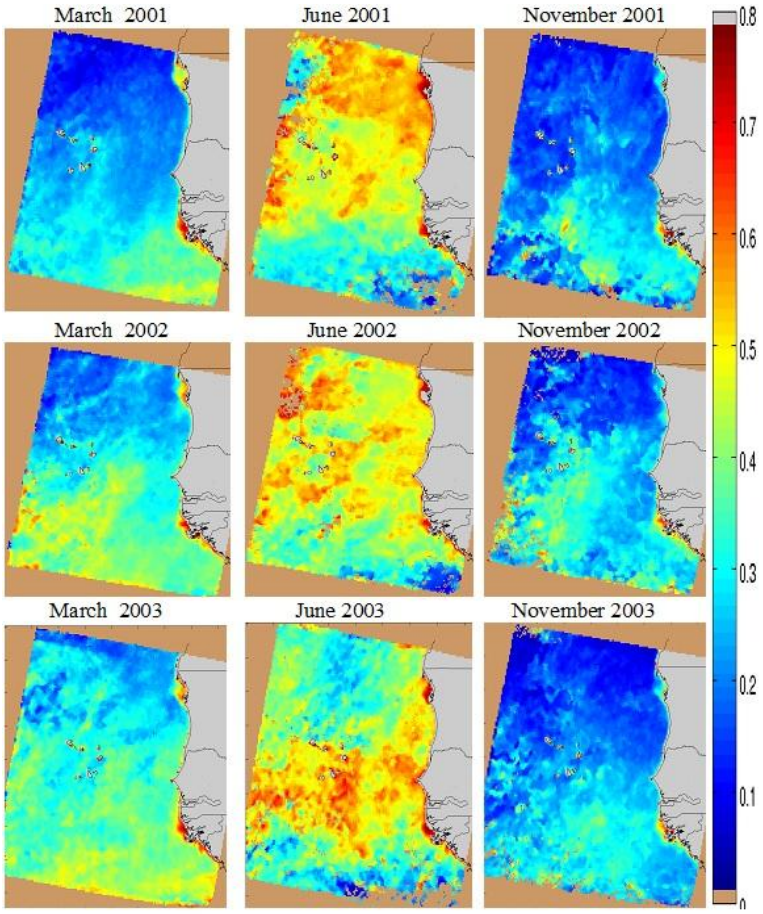

Fig. 4. Spatial distribution of the optical thickness of aerosols. Monthly average of March 2001, 2002 and 2003; June 2001, 2002 and 2003; and November 2001, 2002 and 2003

Wind is the meteorological parameter that is responsible of the movement of aerosols. The action of the wind on the surface oceanic layers, results in the existence of waves that break from a certain critical speed of the wind (of the order of 5 $m.s^{-1}$). In the atmospheric layer above the ocean, the drops of water projected into the air break out, thus releasing fine droplets which are suspended in the atmosphere, in the form of maritime aerosols, and which, because of the turbulence, are distributed in the lower layers of the atmosphere and form the maritime aerosols.

In the Earth atmospheric layer, when the wind exceeds a threshold speed, it sets on the ground small fragments (sands, dust) of the earth crust (saltation phase). Some of these fragments due to this mechanical action burst in contact with the soil (sandblasting phase) and release smaller particles, which form the dust. The latter, under the effect of dynamic turbulence in the atmospheric surface layer, can be suspended in the atmosphere and form the aerosols of the desert dust type (dusts).

In each of the squares in Fig. 5, we calculated the monthly mean of the zonal wind U and the monthly mean of the optical thickness as well as its type (Dust or Non-Dust). An analysis was made to establish the relation between the zonal component U of the wind at 775 hpa and the optical thicknesses. Negative components are winds from East to West.

In area 1, the scatter plots between *AOT* and U are shown in Fig. 7. There is a correlation of -61.98% between *AOT* (dust) and U (Fig. 7b). The separability between the different seasons is low. The highlight of this area is the presence of dust with low optical thickness in winter. Studies have identified the sources of these dusts [19]. Among these are the alluvial plain of Bilma (18 °N, 12 °E) and Faya Largeau (18 °N, 19 °E) which are sources of Saharan dust in West Africa below latitude 15 °N during the winter. These low values could come from one or two causes at a time:

- The long distances traveled by the dust, have seen falling many particles especially the largest ones.
- The most residual of the rainy season would control the residence time of the dust.

Spring, Summer and Winter have all been well represented; Autumn is absent.

In Fig. 7.a, it is quite the opposite, only Autumn and Winter are present for the Non-Dust types. A correlation of - 62.16% between *AOT* (Non-Dust) and U.

In square 2, the correlation is weaker than in square 1 (Fig. 8). It is -49.33% between *AOT* (dust) and U but we notice a better separability between the different seasons (the symbols with same color belong to the same season). There are almost no values in winter.

Table 1. Performance indicators on the Dakar site

	SOM-NV	SeaWiFS
relative error	38.8%	74.54%
Correlation	80.23%	13.45%

Table 2. Performance indicators on the Cap-Vert site

	SOM-NV	SeaWiFS
relative error	40.5%	60.75%
Correlation	82.34%	6.38%

The months of Spring and Summer are the only ones practically observed. The easterly winds are much stronger in summer than in spring involving the highest *AOT*. This is in perfect coherence with the map of dust trajectories in summer where the Tamanrasset plains serve West Africa, in about 16 °N [19].

Fig. 8.a shows the opposite, in seasonal terms, of Fig. 8.b. Non-Dust types appear most often in the Autumn and Winter months. A few months of Spring have appeared but far from the diagonal. With a correlation of -51.41% between *AOT* (Non-Dust) and U, Non-Dust aerosols are subject to high altitude zonal winds.

In square 3, the correlation is -60.32% between *AOT* (dust) and U. There are almost no aerosols in winter. There is almost the same trend as square 2 except that the months of the summer are in strong predominance.

For Non-Dust aerosols, the correlation is 30.65% between *AOT* and U.

The first conclusion noted on the three previous figures (Figs. 7, 8, 9) is that the stronger the East-West wind, the higher the optical thickness.

The fact that we do not observe Saharan dust in autumn in square 1 although the U component of the wind is important is due to the development of vegetation after the rainy season (July, August) which protects the soil from erosion of the wind.

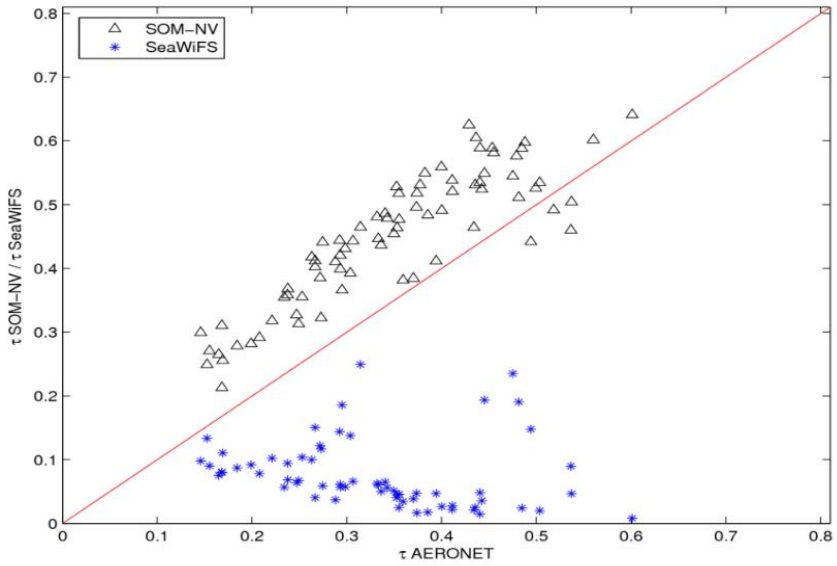

Fig. 5. Scatter plot between monthly mean optical thickness (τ) measurements computed by SOM-NV (Δ) and the SeaWiFS product (*) and the AERONET measurement at Dakar

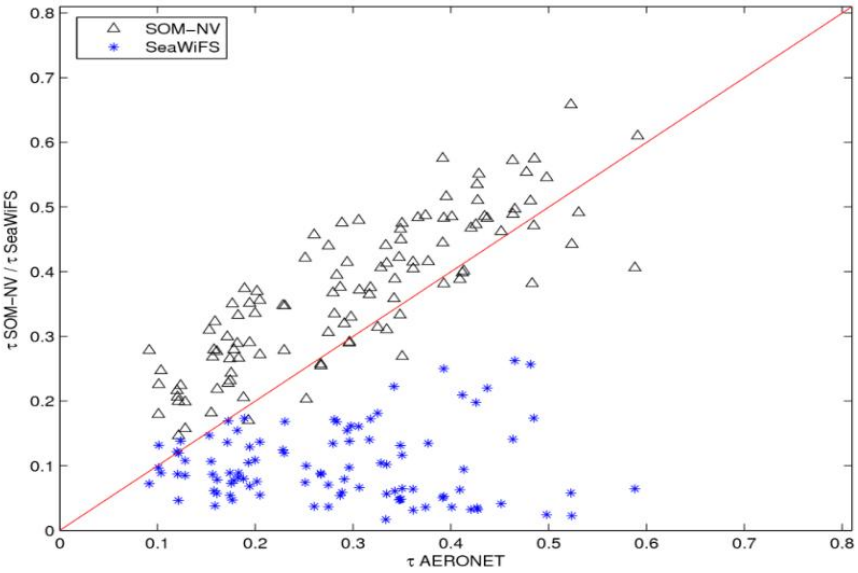

Fig. 6. Scatter plot between monthly mean optical thickness (τ) measurements computed by SOM-NV (Δ) and the SeaWiFS product (*) and the AERONET measurement at Cabo Verde

4.2 Monthly Aerosol Aerosols Types Analysis

The determination of the aerosol type monthly mean is a delicate operation. The aerosol type of each pixel is labellised (Maritime, tropospheric, Oceanic, Coastal, Dust). From level 2 to level 3, the L2 image of 4.5 km resolution is projected onto a L3 grid with a resolution of 9 km. Each box of the L3 grid will contain at most 4 pixels of the L2 image.

The approach used in this work consists in classifying spatially within each box of the L3 grid the pixels into two subsets: "Dusts" and "non-Dusts": the box (or new pixel) of the L3 grid takes the label of the majority set (either "Dust" only or "non-Dust" only). Note that "non-Dusts"

represent the sum of the four types of non-absorbing aerosols. To perform a monthly average, we compare in each box of the grid L3 the number of "Dusts" to "non-Dusts" for one month. (e.g. 30 images of the month). The box is labeled "Dusts" if the detection percentage of the latter is higher than the "non-Dusts" and vice versa. A monthly image labeled "dusts" may therefore contain a significant percentage of "non-dusts" less than 50%.

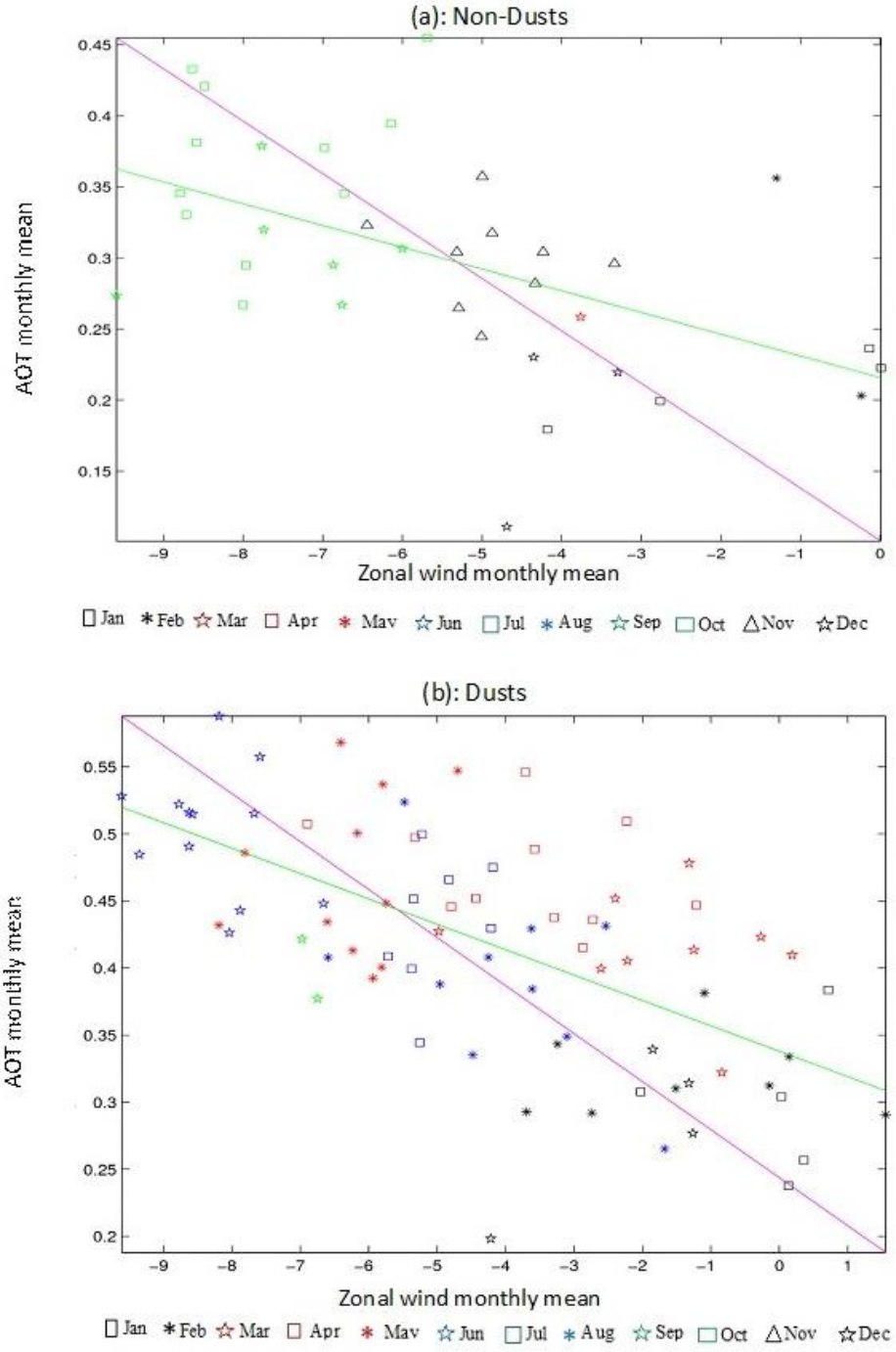

Fig. 7. Scatter plot between zonal wind at 775 hpa U (m/s) and AOT in square 1. Months belonging to the same season are of the same color

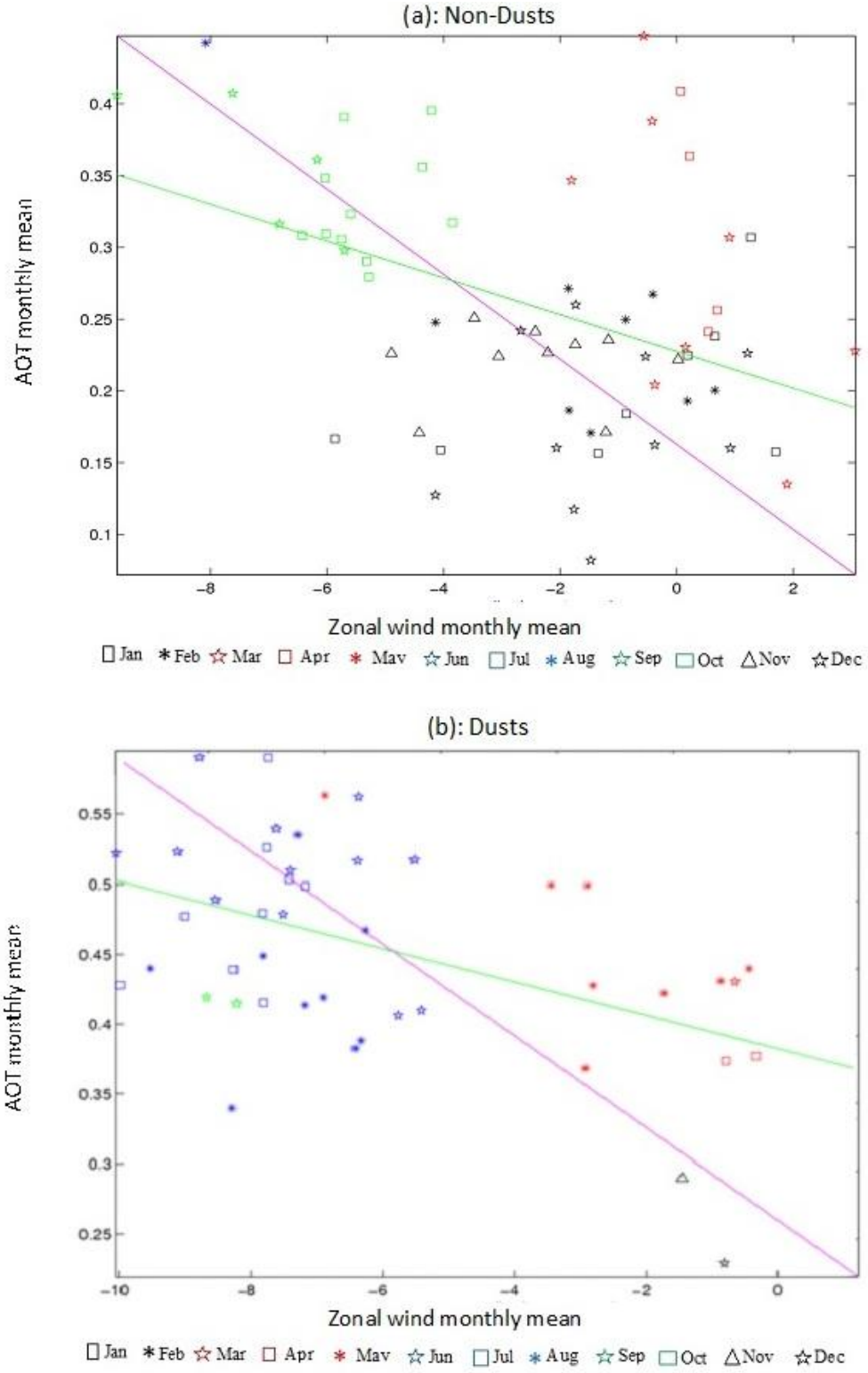

Fig. 8. Scatter plot between zonal wind at 775 hpa U (m/s) and AOT in square 2. Months belonging to the same season are of the same color

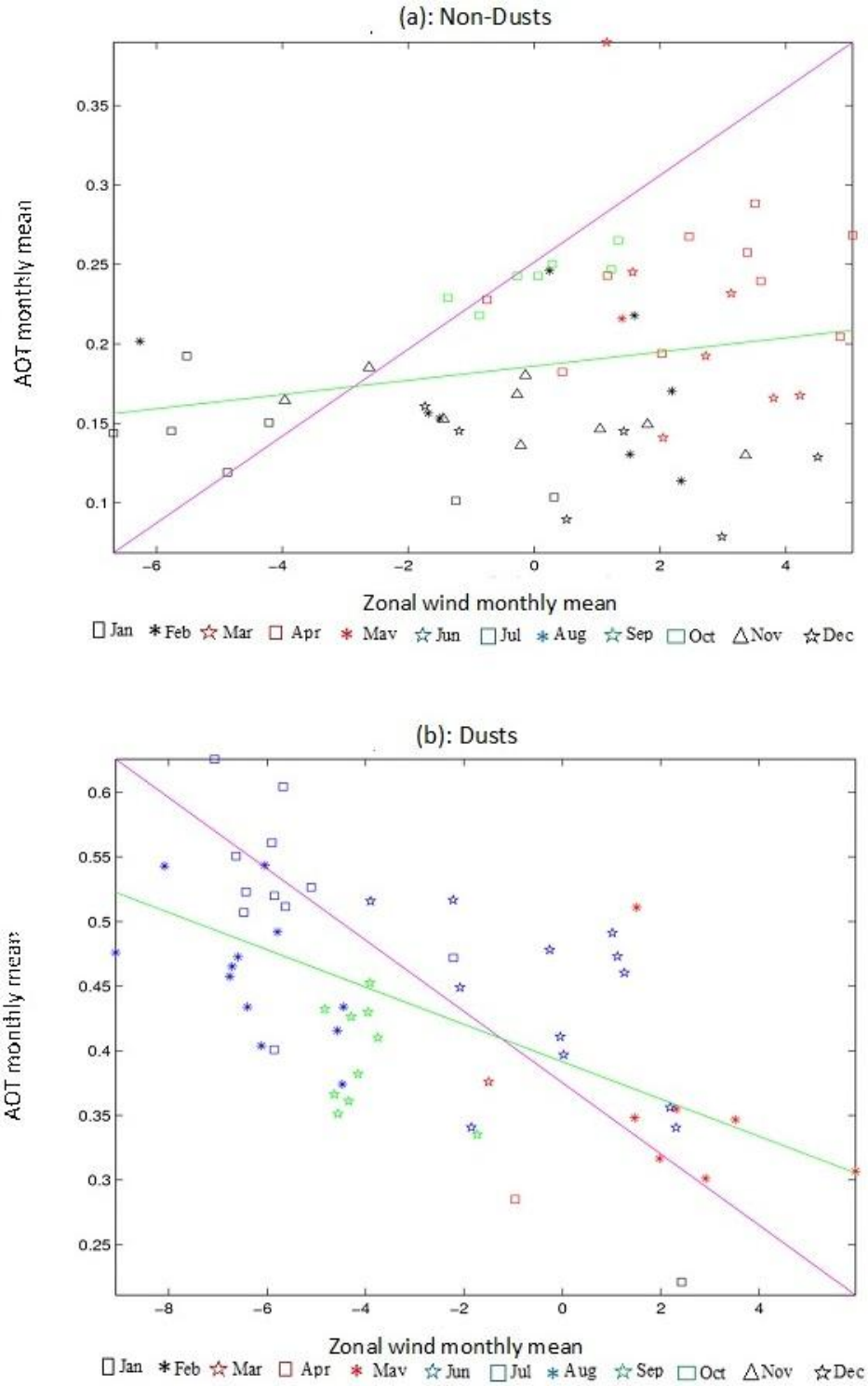

Fig. 9. Scatter plot between zonal wind at 775 hpa U (m/s) and AOT in square 3. Months belonging to the same season are of the same color

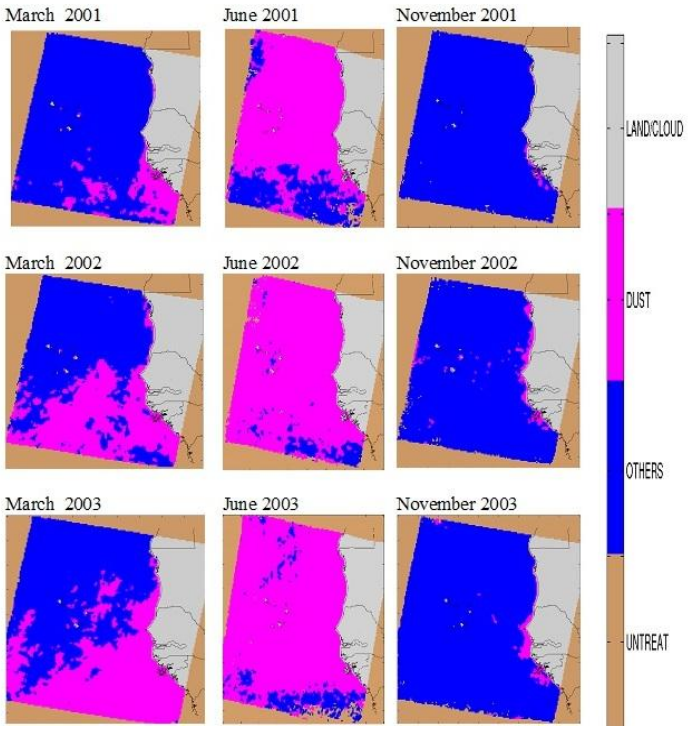

Fig. 10. Spatial distribution of dust: monthly typology of March 2001-2003, June 2001-2003 and November 2001-2003

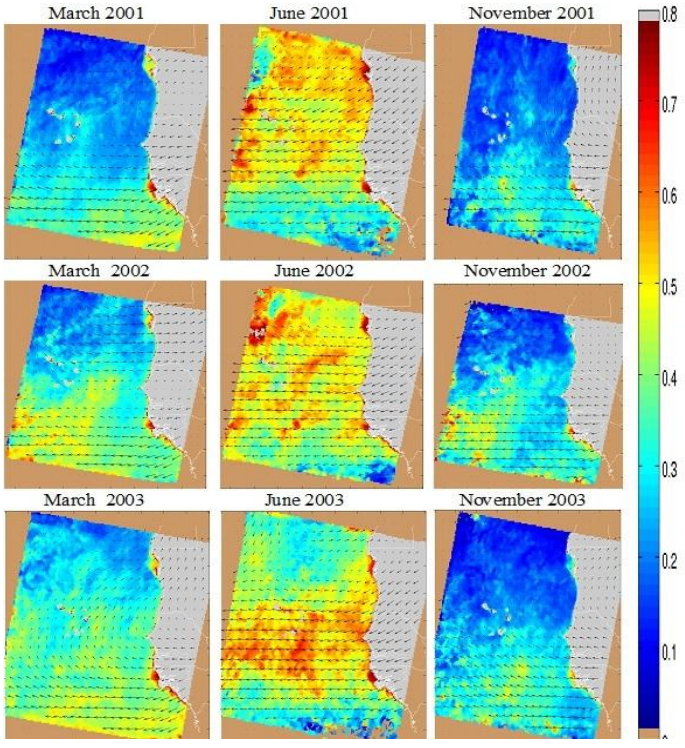

Fig. 11. Spatial distribution of dust: monthly fields of winds at 775 hp from March 2001-2003, June 2001-2003 and November 2001-2003

Fig. 10 shows the monthly events of the aerosol types for the months of March, June and November (2001-2003). Comparing the figure 10 to Fig. 4, we note a certain spatial coherence between the "Dusts" and the high optical thicknesses. During the months of March, the northern part of the image is frequently characterized by non-absorbing aerosols while that of South by dust ("dusts"). In June, the whole image is covered with dust but we observe a tiny part covered with non-absorbing aerosols all the way south. In November the image is completely covered with non-absorbing aerosols, the dust having completely disappeared. Although winds south of 16 °N are often strong and directed westwards, soil moisture and vegetation cover do not allow saltation. Fig. 11 is a repeat of Fig. 4 with a superposition of wind fields at 775 hpa. It brings a double information. First, it confirms everything that has been seen previously and observed about the link between the movement of dust and weather but also confirms that the labeling of aerosol types is good because "Dust" types are linked to strong optical thicknesses and "Non-Dust" to low optical thicknesses.

5. CONCLUSION

The spatial and temporal study of atmospheric parameters detected by inverting SeaWiFS measurements using SOM-NV allowed us to characterize the evolution of these parameters and to show the relations existing between these parameters and certain meteorological variables. From one season to the next, the majority composition of suspended aerosols changes, mainly due to several factors such as the soil moisture and the zonal wind. Thus, it was noticed that desert aerosols covered practically the entire study area around June and almost never exist during the months of November.

COMPETING INTERESTS

Authors have declared that no competing interests exist.

REFERENCES

1. Gordon HR, Wang M. Retrieval of water-leaving radiances and aerosol optical thickness over the oceans with SeaWiFS: A preliminary algorithm. Appied Optics. 1994;33(3):443-453.
2. Husar R, Stowe L, Prospero J. Characterization of tropospheric aerosols over the oceans with NOAA advanced very high resolution radiometer optical thickness operational product. J. Geophys. Res. 1997;102(16):889-909.
3. Moulin C, Lambert CE, Dulac F, Dayan U. Control of atmospheric export of dust from North Africa by the North Atlantic Oscillation. Nature. 1997;387:691-694.
4. Herman JR, Bhartia PK, Torres O, Hsu C, Seftor C, Celarier E. Global distribution of UV-absorbing aerosols from Nimbus 7/TOMS data. Journal of Geophysical Research. 1997;102.
   DOI: 10.1029/96JD03680
   ISSN: 0148-0227.
5. Gordon HR. Atmospheric correction of ocean color imagery in the earth observing system era. Journal of Geophysical Research. 1997;102:17081-17106.
6. Brajard J, Jamet C, Moulin C, Thiria S. Use of a neuro-variational inversion for retrieving oceanic and atmospheric constituents from satellite ocean colour sensor: Application to absorbing aerosols. Neural Networks. 2006;19:178-185.
7. Nobileau D, Antoine D. Detection of blue-absorbing aerosols using infrared and visible (ocean color) remote sensing observations. Remote Sens. Environ. 2005;95(3):368-387.
8. Wang M. Atmospheric correction of ocean color sensors: computing atmospheric diffuse transmittance. Applied Optics. 1999;38(3):451-455.
9. Moulin C, Gordon HR, Banzon VF, Evans RH. Assessment of Saharan dust absorption in the visible from SeaWiFS imagery. J. Geophys. Res. 2001;106: 18239-18250.
10. Wang M, Gordon HR. A simple, moderately accurate, atmospheric correction algorithm for SeaWiFS. Remote Sens. Environ. 100, 82-94. 1994;50(3): 231-239.
11. Shettle EP, Fenn RW. Models of aerosols of the lowers atmosphere and the effect of the humidity variations on their optical properties. Technical Report TR-79- 0214, Air Force Geophysical Laboratory, Bedford, Mass; 1979.
12. Diouf D, Niang A, Brajard J, Crepon M, Thiria S. Retrieving aerosol characteristics and sea-surface chlorophyll from satellite Ocean color multi-spectral sensors using a

neural-variational method. Remote Sens. Environ. 2013;130:74–86.
13. Kohonen T. Self organizing maps (3rd Ed.). Berlin Heidelberg: Springer Verlag. 2001;501.
14. Jamet C, Thiria S, Moulin C, Crepon M. Use of a neuro-variational inversion for retrieving oceanic and atmospheric constituents from ocean color imagery. A feasibility study. Journal of Atmospheric and Oceanic Technology. 2005;22(4):460-475.
DOI: 10.1175/JTECH1688.1
15. Niang A, Gross L, Moulin C, Badran F, Thiria S. Automatic neural classification of ocean colour reflectance spectra at the top of the atmosphere with introduction of expert knowledge. Remote Sens. Environ. 2003;86(2):257-271.
16. Brajard J, Moulin C, Thiria S. Atmospheric correction of SeaWifs ocean colour imagery in the presence of absorbing aerosols of the Indian coast using a neuro-variational method. Geophys. Res. Lett. 2008;35:L20604.
DOI: 10.1029/2008GL035179
17. Bishop C. Neural networks for pattern recognition. Oxford University Press; 1995.
18. Tanre D, Deroo C, Duhaut P, Herman M, Morcrette J, Perbos J, Deschamps PY. Description of a computer code to simulate the satellite signal in the solar spectrum: 5s code. Intern. J. Remote Sens. 1997;11: 659-668.
19. Wilson IG. Desert sandflow basins and a model for the development of ergs. Geogr. J. 1971;137:180-198.

Peer-review history:
The peer review history for this paper can be accessed here:
http://www.sdiarticle4.com/review-history/52971